BIOCHEMISTRY
including biophysical chemistry & molecular biology

Article

pubs.acs.org/biochemistry

# All-Atom Molecular Dynamics Simulations of Actin−Myosin Interactions: A Comparative Study of Cardiac α Myosin, β Myosin, and Fast Skeletal Muscle Myosin

Minghui Li and Wenjun Zheng*

Physics Department, University at Buffalo, Buffalo, New York 14260, United States

Supporting Information

**ABSTRACT:** Myosins are a superfamily of actin-binding motor proteins with significant variations in kinetic properties (such as actin binding affinity) between different isoforms. It remains unknown how such kinetic variations arise from the structural and dynamic tuning of the actin−myosin interface at the amino acid residue level. To address this key issue, we have employed molecular modeling and simulations to investigate, with atomistic details, the isoform dependence of actin−myosin interactions in the rigor state. By combining electron microscopy-based docking with homology modeling, we have constructed three all-atom models for human cardiac α and β and rabbit fast skeletal muscle myosin in complex with three actin subunits in the rigor state. Starting from these models, we have performed extensive all-atom molecular dynamics (MD) simulations (total of 100 ns per system) and then used the MD trajectories to calculate actin−myosin binding free energies with contributions from both electrostatic and nonpolar forces. Our binding calculations are in good agreement with the experimental finding of isoform-dependent differences in actin binding affinity between these myosin isoforms. Such differences are traced to changes in actin−myosin electrostatic interactions (i.e., hydrogen bonds and salt bridges) that are highly dynamic and involve several flexible actin-binding loops. By partitioning the actin−myosin binding free energy to individual myosin residues, we have also identified key myosin residues involved in the actin−myosin interactions, some of which were previously validated experimentally or implicated in cardiomyopathy mutations, and the rest make promising targets for future mutational experiments.

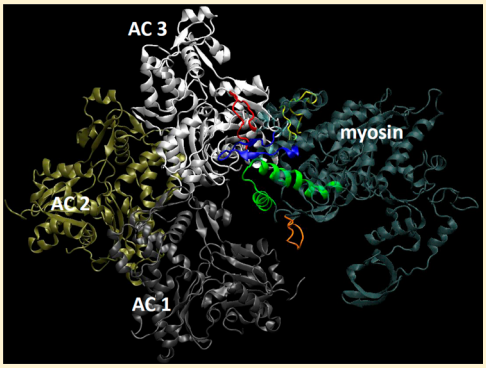


Myosins, a superfamily of motor proteins that move along filamentous actin (F-actin) powered by adenosine triphosphate (ATP) hydrolysis, are involved in many key biological functions ranging from muscle contraction to intracellular transportation. Among at least 20 classes,[1] class II myosins (including various isoforms of muscle and non-muscle myosins) have been intensively investigated for decades via biochemical, biophysical, genetic, and structural studies.[2−4] Despite the overall conservation of the ATPase cycle, the kinetic parameters vary greatly among myosin isoforms;[5] some are slow motors that spend most of the time strongly bound with F-actin, while others are fast motors that spend most of the time weakly bound with (or detached from) F-actin. To study the functional diversity of myosins, it is essential to determine the molecular basis for such kinetic differences between myosin isoforms and how they relate to the tuning of actin−myosin interactions at the amino acid residue level. A primary rationale for studying the kinetics of muscle myosins is that the kinetic properties (including various reaction rates and binding constants) are closely related to the contractile function of muscles, so the kinetic studies promise to illuminate the molecular mechanisms of mutations that cause muscle diseases such as hypertrophic cardiomyopathy (HCM) (for a review, see ref 6).

As an important example for functional differences entailed by kinetic differences in myosins, there are two major isoforms of cardiac myosin in human heart, cardiac α and β myosin (denoted Cα and Cβ, respectively), which are highly similar in amino acid sequence (91% identical). The Cβ isoform has been of special interest because of its prominent role in a series of cardiomyopathies.[7] The relative proportions of these two isoforms vary in response to different physiological stimuli [such as disease, exercise, and hormonal status (see refs 8 and 9)]. To explore the kinetic basis for the functional differences between these two isoforms, a recent kinetic study of human Cα and Cβ isoforms revealed substantial differences in individual kinetic parameters, overall contractile character, and predicted cycle times.[10] For these parameters, the Cα isoform is more similar to the fast skeletal muscle myosin (denoted FSk) than to the Cβ isoform. In particular, the actin binding affinity of the Cα isoform is 5−10-fold weaker than that of the Cβ isoform but similar to that of the FSk isoform (within 2-fold).[10] It remains unclear how the kinetic differences

**Received:** May 30, 2013
**Revised:** October 24, 2013
**Published:** October 29, 2013





dx.doi.org/10.1021/bi4006896 | *Biochemistry* 2013, 52, 8393−8405

among the Cα, Cβ, and FSk isoforms originate from their sequential and structural differences despite recent studies.[10−12]

Because of decades of efforts, many high-resolution X-ray structures of myosins have been determined in the absence of actin, which are either bound with nucleotide analogues (corresponding to weak actin-binding states)[5,13−17] or without nucleotides (corresponding to a strong actin-binding or rigor-like state).[18−21] However, no X-ray structure of the actin−myosin complex has been determined to date. As an alternative approach to study the structural basis of actin−myosin interactions, a number of actomyosin models have been built by docking the myosin X-ray structure and F-actin model[22−24] into cryo-electron microscopy (cryo-EM) maps of myosin-decorated F-actin.[25−30] Because of the improving resolutions of EM maps in recent years, these EM-based actomyosin models have offered increasingly detailed views of actin−myosin interactions in the rigor state.[31]

The actin−myosin interactions are highly dynamic, involving various flexible loops at the actomyosin interface.[32] Therefore, it is essential to probe the actomyosin dynamics with high spatial and temporal resolutions. To this end, computer-based molecular dynamics (MD) simulations have proven to be useful in complementing experimental studies of myosin function.[33−38] The EM-based actomyosin models have provided good initial models for all-atom MD simulations to explore the dynamic interactions between actin and myosin. Two previous studies of actin−myosin interactions were performed for chicken FSk myosin based on relatively short MD simulations (up to 5 ns), one with implicit solvent[37] and the other with the constraints of an EM map.[32] These studies have yielded unprecedented details of the actin−myosin interface and established MD as a useful approach for exploring actin−myosin interactions. However, it remains unknown if MD simulations, limited to nanosecond time scales by modern computing power, are capable of probing the subtle differences in actin−myosin interactions between different myosin isoforms.

To meet the challenge described above, we have performed extensive all-atom MD simulations with explicit solvent to probe the isoform dependence of actin−myosin interactions in the rigor state. By combining EM-based docking with homology modeling (see Methods), we have constructed three all-atom models for human Cα, Cβ, and rabbit FSk myosin in complex with three actin subunits in the rigor state. Starting from these three models, we have performed, to the best of our knowledge, the most extensive all-atom MD simulations to date (total of 100 ns per system) and then used the MD trajectories to calculate the actin−myosin binding free energy with contributions from both electrostatic and nonpolar forces. Our binding calculations are in good agreement with the experimental finding of isoform-dependent actin binding affinity in the following order: FSk < Cα < Cβ. Such isoform-dependent differences are traced to changes in actin−myosin electrostatic interactions (e.g., hydrogen bonds and salt bridges) involving several highly flexible actin-binding loops. By partitioning the actin−myosin binding free energy to individual myosin residues, we have also identified key myosin residues involved in the actin−myosin interactions, some of which were previously identified experimentally or implicated in cardiomyopathy mutations, and the rest make promising targets for future mutational experiments.

This study has demonstrated the feasibility of using MD simulations to explore subtle differences in actin−myosin interactions between various myosin isoforms, which will lead to novel structural and dynamic insights into the kinetic differences between Cα and Cβ isoforms[10] and how their functions are perturbed by disease-causing mutations.[39]

## METHODS

**Preparation of Models.** We built a homology model of the chicken fast skeletal muscle (chkFSk) myosin motor domain [residues 1−779, except loop 2, residues 627−646, to be added later (see below)] with MODELER,[40−42] using a rigor-like X-ray structure of squid myosin (PDB entry 3I5G)[21] as the template. 3I5G was chosen as the template because it has the highest resolution among the three rigor-like X-ray structures of myosin with a sequence 61−62% identical to that of chkFSk (the PDB entries of the two other structures are 2OS8 and 2EC6). The sequence of chkFSk was obtained from the NCBI database (P13538.4). Five homology models were generated by MODELER, and the one with the lowest DOPE score was chosen as the initial model of chkFSk.

Then we used Chimera[43] to fit the model of chkFSk described above and a five-actin model from ref 30, as two rigid bodies, into a cryo-EM map of myosin-decorated F-actin at 13 Å resolution.[29] We further used the sequential fitting function of Chimera to optimize the EM-fitted actomyosin model by reducing the number of atomic clashes between actin and myosin.

The missing loop 2 (residues 626−642) in 3I5G is involved in strong actin binding as shown by a loop 2 deletion experiment,[44] so it cannot be reliably modeled by MODELER for myosin in the absence of actin. We used an in-house program to model the Cα trace of loop 2 as follows: starting from residue 626 and 647 of chkFSk, we grow the N-terminal and C-terminal parts of loop 2 separately as two random coils toward residue 2 of the third actin subunit (named AC3), so that the "merged" loop 2 extends toward and interacts with the N-terminal acidic residues of AC3. Such interactions are implicated by previous mutational, antibody binding, and cross-linking experiments[45−47] and were previously used to constrain the dynamic docking of myosin and actin.[48] One hundred models of loop 2 were generated and evaluated by the electrostatic interaction energy between the basic residues of loop 2 and acidic residues D1, E2, D3, E4, D24, D25, E99, and E100 of AC3, which were experimentally implicated in myosin binding.[45,46,49] The loop 2 model with the lowest electrostatic energy was chosen. Then we used the complete command of MMTSB[50] to add non-Cα backbone atoms and side-chain atoms to the Cα trace of loop 2.

On the basis of the chkFSk model described above as a template, we used MODELER to build three homology models for the motor domains of three myosin isoforms, human Cβ myosin (abbreviated humCβ, residues 1−783), human Cα myosin (abbreviated humCα, residues 1−785), and rabbit FSk myosin (abbreviated rabFSk, residues 1−780). The amino acid sequences were obtained from the NCBI database (P12883.5, BAA00791.1, and AAA74199.1, respectively). The sequences of humCβ, humCα, and rabFSk are 80, 80, and 89% identical with that of chkFSk, respectively. To preserve the backbone conformation at the actin−myosin interface, we used the mutator function of VMD[51] to separately model the side-chain coordinates of four highly conserved actin-binding loops, loop 3, loop 4, the cardiomyopathy loop (CM loop), and the C-terminal part of loop 2 (see Table S1 of the Supporting Information). By combining these three homology models with

the five actin subunits from the EM-fitted actomyosin model of chkFSk, we have constructed three actomyosin models for humC$\beta$, humC$\alpha$, and rabFSk. Because these models were based on the same rigid EM fitting step, no global structural differences between them have been introduced because of the limited EM resolution.

**MD Simulation.** To reduce the computational cost for MD simulation, we kept three actin subunits (named AC1−AC3), with AC1 and AC3 directly interacting with myosin (see Figure 1). The hydrogen atoms were added with VMD.[51] Each

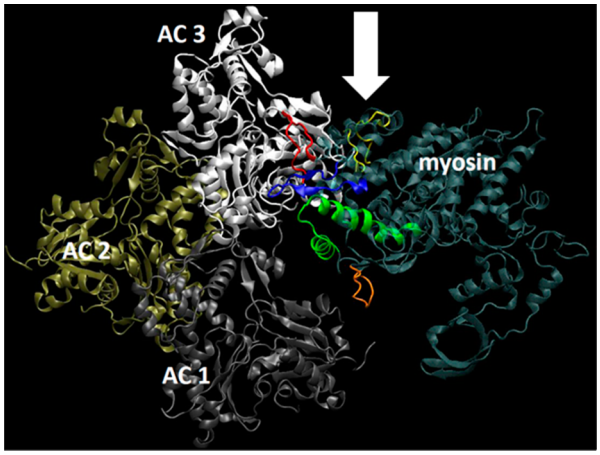


**Figure 1.** Rigor-state complex of three actin subunits (AC1−AC3) and the chkFSk myosin motor domain with the actin-binding motifs colored as follows: blue for loop 4, red for the CM loop, orange for loop 3, yellow for loop 2, and green for the HLH motif.

actomyosin model was immersed in a rectangular box of water molecules extending up to 10 Å from the proteins in each direction by using VMD. To ensure an ionic concentration of 150 mM and zero net charge, $Na^+$ and $Cl^-$ ions were added to each system using VMD. After solvation and ionization, each system has a total of ∼250000 atoms.

To adequately explore the dynamics of actin−myosin interactions, we performed 10 independent MD simulations for each of the three systems described above. First, a 5000-step energy minimization was conducted using the steepest descent method with harmonic restraints (force constant of 5 kcal $mol^{-1}$ $Å^{-2}$) applied to all protein backbone atoms, followed by a 5000-step energy minimization with harmonic restraints (force constant of 1 kcal $mol^{-1}$ $Å^{-2}$) applied to all protein backbone atoms except loops 2−4 and the CM loop of myosin and N-terminal residues 1−4 of actin. Next, the systems were heated to 300 K over 100 ps with the same harmonic restraints as in the first minimization. Then, a 500 ps equilibration run was performed in the *NVT* ensemble with the same harmonic restraints that were used in heating. Finally, the systems were subjected to a 10 ns MD simulation performed in the *NPT* ensemble with weak harmonic restraints (force constant of 0.01 kcal $mol^{-1}$ $Å^{-2}$) applied to all protein backbone atoms except loops 2−4 and the CM loop of myosin and N-terminal residues 1−4 of actin. The Nosé−Hoover method[52] was used with a temperature of 300 K and a pressure of 1 atm. The periodic boundary conditions were applied to the systems. A 10 Å switching distance and a 12 Å cutoff distance were used for nonbonded interactions. The particle mesh Ewald method[53] was used to calculate long-range electrostatic interactions. The SHAKE algorithm[54] was used to constrain bond lengths of hydrogen-containing bonds, which allowed a time step of 2 fs for MD simulations. The coordinates of the systems were saved every 2 ps during the MD simulations for later analyses. Energy minimization and MD simulation were conducted using NAMD version 2.9b2[55] with the CHARMM27 force field[56] and TIP3P water model.[57]

**Hydrogen Bond Analysis.** We used the following geometric criteria to identify a hydrogen bond (HB) between two N/O/S atoms (i.e., acceptor and donor): a donor−acceptor distance of <3.5 Å and a donor−hydrogen−acceptor angle of <60°.[58] For ten 10 ns MD trajectories of each system, we saved 100 frames of the last 2 ns of each trajectory and then combined them to form a structural ensemble of a total of 1000 frames. Then we used VMD[51] to identify and calculate the occupancies of all HBs between AC1/AC3 and myosin within this ensemble. The occupancies of HBs between the same pair of residues were added, so their values may exceed 1 for some residue pairs.

**Salt Bridge Analysis.** We used the following criteriion to identify a salt bridge (SB) between two oppositely charged residues: a maximal distance of 4 Å between two charged atoms (oxygen or nitrogen).[59] We used VMD[51] to identify and calculate the occupancies of all SBs between AC1/AC3 and myosin within the 1000-frame ensemble (see above). The occupancies of SBs between same pair of residues were added.

**Calculation of the Actin−Myosin Binding Free Energy.** Following our previous papers,[60,61] we calculated the actin−myosin binding free energy $\Delta G$ for three systems (humC$\alpha$, humC$\beta$, and rabFSk). We extracted 100 frames of the last 2 ns of each MD trajectory after stripping all waters and ions and then calculated $\Delta G$ for each frame and averaged $\Delta G$ over all 1000 frames from 10 trajectories. Following a continuum solvent model,[62] $\Delta G$ was empirically expressed as $\Delta G = \Delta G_{np} + \Delta G_{elec}$. Here the nonpolar contribution $\Delta G_{np}$ ($=\alpha E_{vdW}$) was empirically written as a fraction ($\alpha < 1$) of the van der Waals (vdW) interaction energy ($E_{vdW}$) between myosin and AC1/AC3, and the electrostatic contribution $\Delta G_{elec}$ ($=\beta \Delta E_{elec}$) was empirically written as a fraction ($\beta < 1$) of the change in electrostatic energy ($\Delta E_{elec}$) from unbound myosin and actin to the actomyosin complex. Electrostatic energy $E_{elec}$ was calculated using the Poisson−Boltzmann (PB) method.[63,64] An $\alpha$ of 0.158 and a $\beta$ of 0.153 were obtained by fitting the kinesin−microtubule binding data from an alanine-scanning mutagenesis study.[60] These parameters are transferred to actin−myosin binding because kinesin and myosin are structurally related[65] and have chemically similar binding interfaces with the corresponding polymeric tracks (i.e., microtubule and F-actin). For the PB calculation,[63,64] a dielectric constant $\varepsilon_i$ of 4 was used for the protein interior.[66−69] A dielectric constant $\varepsilon_e$ of 80 was used for the exterior aqueous environment. A probe radius of 1.4 Å was used to define the molecular surface corresponding to the dielectric boundary. The salt concentration was set to 0.12 M, corresponding to the buffer condition for binding measurements.[10,70] All the PB calculations were performed using the PBEQ module[64,71,72] of CHARMM.[73] The atomic Born radii used here were previously calibrated and optimized to reproduce the electrostatic free energy of the 20 amino acids in MD simulations with explicit water molecules.[72]

Next, we used CHARMM to partition $\Delta G$, $E_{vdW}$, and $\Delta E_{elec}$ to contributions from individual myosin residues [denoted $\Delta G_n$, $E_{vdW,n}$, and $\Delta E_{elec,n}$ for residue $n$ (for details see refs 60 and 61 and analys.doc and pbeq.doc at http://www.charmm.


dx.doi.org/10.1021/bi4006896 | *Biochemistry* 2013, 52, 8393−8405

org/documentation/c37b1/index.html)]. Then we ranked all myosin residues by $|\Delta G_n|$ and kept the top 5%, which were predicted to be important to actin−myosin binding. The choice of 5% corresponds to a $p$ value of 0.05 (i.e., the probability that a random ranking of all myosin residues would place a given residue in the top 5%), which is widely used as the standard significance level.[74]

**Estimation of the Experimental Actin−Myosin Binding Free Energy.** We used the following dissociation constants ($K_d$) as measured previously under the nucleotide-free condition (with 100 mM NaCl/KCl buffer at 20 °C): 71 nM for rabFSk,[70] 37 nM for humC$\alpha$,[10] and 8 nM for humC$\beta$.[10] We estimated the actin−myosin binding affinity at the same ionic concentration (0.12 M) using the equation $\Delta G_{exp} = k_B T \ln(K_d)$ (where $T$ = 20 °C and $k_B$ is Boltzmann's constant) and obtained values of −9.6 kcal/mol for rabFSk, −10.0 kcal/mol for humC$\alpha$, and −10.9 kcal/mol for humC$\beta$.

## RESULTS AND DISCUSSION

**Construction of Models Based on EM Fitting.** By using EM-based rigid fitting and homology modeling, we have built an actomyosin model for chkFSk in the rigor state starting from a rigor-like X-ray structure of myosin and a five-actin model (see Methods). After rigid fitting, both the myosin motor domain and five actin subunits fit well into the 13 Å EM density map of myosin-decorated F-actin,[29] except for some surface loops near the actin−myosin interface [such as loop 3 and loop 4 of myosin (see Figure S1 of the Supporting Information)] and elsewhere [such as loop 1 of myosin (see Figure S1 of the Supporting Information)]. In a recent study, Lorentz and Holmes modeled the actomyosin complex for chkFSk by performing an MD-based flexible fitting of the same EM map,[29] which allowed conformational changes within myosin and actin during fitting.[32] We chose not to perform flexible fitting because the quality of our rigid fitting is already comparable to that of the flexible fitting in ref 32, especially for the myosin densities (see Table S2 of the Supporting Information). Therefore, we infer that the rigor-like X-ray structure of myosin does not undergo large conformational changes upon forming the strong-binding actomyosin complex in the rigor state. Nevertheless, as indicated by the rigid fitting result (see Figure S1 of the Supporting Information), several actin-binding loops (including loops 2−4 and the CM loop) may change structurally and dynamically in response to actin binding, which will be further explored by MD simulations (see below).

On the basis of the EM-fitted actomyosin model of chkFSk (see Figure 1), we have modeled the missing loop 2 as two random coils merged together with optimized electrostatic interactions with several acidic residues of AC3 experimentally implicated in actin−myosin binding (see Methods). Such experimentally constrained modeling and optimization is necessary because loop 2 contributes significantly to actin−myosin binding,[44] and it is too long (~20 residues) for other loop modeling methods.

After adding loop 2, we have used homology modeling to build three actomyosin models for three myosin isoforms (rabFSk, humC$\alpha$, and humC$\beta$) in the rigor state (see Methods). Because of the high level of sequence identity (80−89%) between these isoforms and chkFSk, the resulting homology models are highly similar, especially at the actin−myosin interface. Therefore, it is not obvious what is the structural origin for their different actin binding affinities in the rigor state.[10]

**MD Simulations and Flexibility Analysis.** To explore the dynamic interactions between myosin and three actin subunits [AC1−AC3 (see Figure 1)] in the rigor state, we have performed ten 10 ns MD simulations with explicit solvent (see Methods), which start from the three actomyosin models of humC$\beta$, humC$\alpha$, and rabFSk. This endeavor is, to the best of our knowledge, the most extensive MD simulation of actin−myosin interactions reported to date.

To assess how well the systems are equilibrated during the MD simulations, we have analyzed the root-mean-square deviation (rmsd) of backbone atoms (relative to the initial actomyosin models) for each MD trajectory (see Figure S2 of the Supporting Information). For all three systems, the rmsd rapidly increases and starts to saturate within the first 2 ns and then stabilizes near 2 Å during the remaining 8 ns (see Figure S2 of the Supporting Information). Interestingly, we have observed some differences in rmsd among the three systems. For the last 2 ns of 10 MD trajectories, the rmsd values are 1.8−2.2, 1.9−2.3, and 1.9−2.4 Å for humC$\beta$, humC$\alpha$, and rabFSk, respectively. By comparing the rmsd values and their variations between trajectories (see Figure S2 of the Supporting Information), we have found that rabFSk is the most flexible, while humC$\beta$ is the least flexible among the three isoforms. Such isoform dependence in flexibility may be related to the differences in actin binding affinity among rabFSk, humC$\alpha$, and humC$\beta$: the higher flexibility of rabFSk may be caused by the formation of a less stable actin−myosin complex with a lower binding affinity (see below).

Both F-actin and myosin are flexible biomolecules, so it is not appropriate to treat F-actin as a rigid body fixed in space during MD simulations. On the other hand, we should also consider the restraining effect of the rest of F-actin on the three actin subunits (AC1−AC3) included in our MD simulations. Therefore, to properly control the flexibility of AC1−AC3 in our MD simulations, we have imposed weak positional restraints (using harmonic springs with a force constant of 0.01 kcal mol$^{-1}$ Å$^{-2}$) on the C$\alpha$ atoms of actin residues excluding the highly flexible N-terminal residues 1−4.[75,76] To calibrate the actin flexibility entailed by such restraints, we have calculated the average rmsd for AC1−AC3 (relative to the initial models) during the last 2 ns of all MD trajectories, which yield rmsd values of 1.8−2.1 Å (see Table S3 of the Supporting Information). For comparison, we have calculated the rmsd between the flexibly fitted actin models obtained in two EM-fitting studies[31,32] and the initial actin models [PDB entries 2ZWH and 3MFP (see refs 23 and 24)], which gave similar rmsd values of 1.9−2.2 Å. Additionally, the rmsd between two recent actin models (PDB entries 2ZWH and 3MFP) is also 2 Å. Therefore, the internal flexibility of actin subunits depicted in our MD simulations is consistent with previous modeling studies of F-actin based on state-of-the-art structural data.[23,24]

To properly describe the flexibility of myosin in our MD simulations, we have applied the same weak positional restraints to myosin residues [except for four flexible actin-binding loops (see Figure 1)]. As observed in a recent EM-fitting study, myosin shows conformational flexibility even when it is strongly bound to F-actin in the rigor state.[31] Indeed, the myosin models obtained by EM-based flexible fitting differ by an rmsd of 2.1−2.6 Å,[31] which is comparable to the average rmsd of 2−2.3 Å for myosin observed during the last 2 ns of all MD trajectories (see Table S3 of the Supporting Information). Therefore, the internal flexibility of myosin depicted in our MD

simulations is comparable with that observed in the recent EM-fitting study.[31]

To further compare the flexibility of the actin−myosin interface among the three myosin isoforms, we have performed root-mean-square fluctuation (rmsf) analysis based on the last 2 ns of MD simulations for three systems. Because the rmsf analysis is based on the parts of MD trajectories obtained after equilibration, it allows us to focus on the differences in flexibility among the three myosin isoforms instead of the isoform-dependent structural rearrangements that optimize or equilibrate the actin−myosin interface. The four actin-binding loops [loops 2−4 and the CM loop (see Figure 1)] are highly flexible [corresponding to peaks in the rmsf plot (see Figure 2)]. Among these loops, loop 2 is the most flexible with the highest rmsf (see Figure 2). Interestingly, we have observed some differences in the rmsf among the three systems: humC$\beta$ has the lowest rmsf in actin-binding loops (particularly in loop 3), while rabFSk has the highest rmsf (especially in loops 2 and 3). Taken together with the rmsd results (see Figure S2 of the Supporting Information), we have found that rabFSk is more flexible than humC$\beta$ in terms of both the global structure and the actin-binding interface, which may be linked to the differences in actin binding affinity between rabFSk and humC$\beta$.[10] For a detailed view of the structural variations in those actin-binding loops as sampled by MD simulations, see Movie S1 of the Supporting Information.

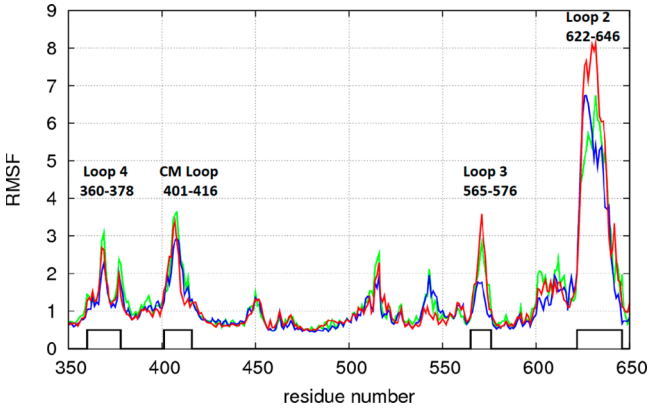


**Figure 2.** Comparison of rmsf values of humC$\alpha$ (green), humC$\beta$ (blue), and rabFSk (red). The residue ranges of four actin-binding loops (loops 2−4 and the CM loop) are labeled (using residue numbers of humC$\beta$). The residue numbers of humC$\alpha$ and rabFSk are shifted to align with those of humC$\beta$ in sequence. rmsf is in angstroms.

**Actin−Myosin Binding Calculations.** On the basis of extensive MD simulations, we have performed intermolecular binding calculations between myosin and two actin subunits [AC1 and AC3 (see Figure 1)] using an empirical protocol (see Methods), which takes into account both electrostatic and nonpolar contributions to the actin−myosin binding free energy (denoted as $\Delta G$). We have recently applied this protocol to the binding interactions between the kinesin motor and microtubule in three biochemical states.[60,61] This protocol was shown to be sufficiently accurate and sensitive to probe the changes in binding affinities between different biochemical states and by alanine scanning mutagenesis.[60,61]

A comparison of the electrostatic contribution [denoted $\Delta E_{elec}$ (see Methods)] indicates humC$\beta$ forms the strongest electrostatic interaction with actin [$\Delta E_{elec} \sim -28.9 \pm 6.3$ kcal/mol (see Figure 3a)], followed by humC$\alpha$ [$\Delta E_{elec} \sim -25.1 \pm 4.7$ kcal/mol (see Figure 3b)] and rabFSk [$\Delta E_{elec} \sim -22.8 \pm 4.3$ kcal/mol (see Figure 3c)], which is in good agreement with the order of actin binding affinity measured experimentally [humC$\beta$ > humC$\alpha$ > rabFSk (see Methods)]. However, the nonpolar contribution [denoted as $E_{vdW}$ (see Methods)] is very close between humC$\beta$ ($E_{vdW} \sim -148.0 \pm 16.1$ kcal/mol (see Figure 3a)] and humC$\alpha$ [$E_{vdW} \sim -149.1 \pm 15.1$ kcal/mol (see Figure 3b)], while rabFSk has the lowest $E_{vdW}$ [$E_{vdW} \sim -140.9 \pm 15.7$ kcal/mol (see Figure 3c)]. Despite large fluctuations in $\Delta E_{elec}$ and $E_{vdW}$ as indicated by the standard deviations (sd) in Figure 3, the differences between isoforms described above are statistically significant because of greatly reduced standard errors ($\sim$sd/$\sqrt{1000}$ due to averaging over 1000 structural frames). Taken together, the observations of different actin binding affinity between these myosin isoforms can be largely attributed to the differences in actin−myosin electrostatic interaction between them. This finding supports the importance of electrostatic forces in tuning actin−myosin binding in various myosin isoforms. Additionally, the stronger electrostatic interaction in humC$\beta$ is accompanied by larger variations in $\Delta E_{elec}$ (see Figure 3), which supports the key role of dynamics in tuning actin−myosin interactions.

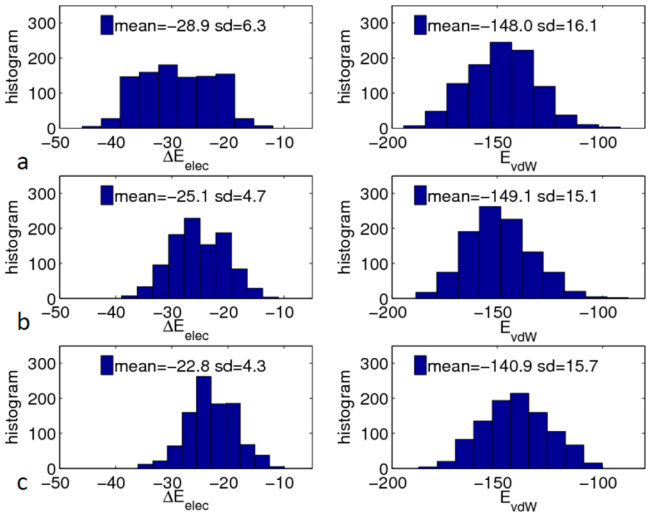


**Figure 3.** Distribution of the electrostatic contribution ($\Delta E_{elec}$) and nonpolar contribution ($E_{vdW}$) to the actin−myosin binding free energy for (a) humC$\beta$, (b) humC$\alpha$, and (c) rabFSk. The binding calculations were performed for 1000 frames taken from the last 2 ns of 10 MD simulations for each system. The energy values are in units of kilocalories per mole; the mean and standard deviation (sd) are shown for each distribution.

We note that the calculated $\Delta G$ values ($-27.8 \pm 2.8$, $-27.4 \pm 2.4$, and $-25.8 \pm 2.6$ kcal/mol for humC$\beta$, humC$\alpha$, and rabFSk, respectively) are not comparable with the experimentally deduced $\Delta G_{exp}$ values from binding measurements [$-10.9$, $-10.0$, and $-9.6$ kcal/mol for humC$\beta$, humC$\alpha$, and rabFSk, respectively (see Methods)], because the entropic cost of actin−myosin binding (corresponding to the differences between $\Delta G_{exp}$ and $\Delta G$) is not taken into account because of the large uncertainty in the entropy calculation. Despite such a caveat, our binding calculations have roughly reproduced the 1−2 kcal/mol differences in actin binding affinity between these myosin isoforms. Future method development will be needed to accurately estimate the entropic contribution to actin−myosin binding. Given our finding of higher flexibility in rabFSk than in the other two isoforms, the entropic cost is


dx.doi.org/10.1021/bi4006896 | Biochemistry 2013, 52, 8393−8405

**Table 1. Distribution of Actin−Myosin Binding Free Energy among Actin-Binding Motifs**

| | | average (sd) of the energy contribution (kcal/mol) | | | percentage | |
|---|---|---|---|---|---|---|
| isoform | energy term | loop 4 | CM loop | HLH motif | loop 3 | loop 2 |
| rabFSk | $E_{vdW}$ | −1.2 (4.0), 1% | −33.7 (4.5), 24% | −53.2 (6.8), 38% | −8.6 (5.5), 6% | −34.4 (6.8), 24% |
| | $\Delta E_{elec}$ | −4.2 (2.3), 17% | −3.7 (2.0), 15% | 1.2 (2.9), 0% | −10.3 (4.5), 42% | −6.8 (3.9), 28% |
| | $\Delta G$ | −0.8 (0.6), 3% | −5.9 (0.8), 23% | −8.2 (1.1), 32% | −2.9 (0.9), 11% | −6.5 (1.2), 25% |
| humC$\alpha$ | $E_{vdW}$ | 0.1 (3.6), 0% | −35.8 (6.0), 24% | −54.6 (6.0), 37% | −6.1 (4.3), 4% | −41.9 (6.7), 28% |
| | $\Delta E_{elec}$ | −4.7 (2.1), 18% | −4.5 (2.4), 17% | 0.3 (2.2), 0% | −7.6 (3.1), 28% | −8.1 (4.0), 30% |
| | $\Delta G$ | −0.7 (0.6), 3% | −6.3 (1.0), 23% | −8.6 (1.0), 31% | −2.1 (0.8), 8% | −7.9 (1.2), 28% |
| humC$\beta$ | $E_{vdW}$ | −0.7 (3.4), 0% | −42.3 (5.9), 29% | −49.5 (7.8), 33% | −4.8 (4.9), 3% | −40.4 (7.4), 27% |
| | $\Delta E_{elec}$ | −4.0 (2.1), 13% | −4.2 (2.9), 14% | 0.4 (2.7), 0% | −8.7 (3.9), 29% | −10.2 (4.2), 34% |
| | $\Delta G$ | −0.7 (0.5), 3% | −7.3 (1.0), 26% | −7.8 (1.3), 28% | −2.1 (0.8), 7% | −7.9 (1.2), 28% |

expected to be lower for rabFSk than for the other two isoforms. Therefore, the differences in entropic contribution cannot account for the observation of weaker actin binding for rabFSk than humC$\beta$ and humC$\alpha$.

To assess the relative contribution to actin−myosin binding from individual actin-binding motifs [including loops 2−4, the CM loop, and the HLH motif (see Figure 1 and Table S1 of the Supporting Information)], we have partitioned $\Delta G$ and its electrostatic and nonpolar contributions to each motif for three myosin isoforms (see Table 1).

For nonpolar contribution $E_{vdW}$, the HLH motif contributes the most in all three isoforms, followed by the CM loop and loop 2 (see Table 1); together they form the main hydrophobic interface between actin and myosin. In comparison, loops 3 and 4 contribute much less to $E_{vdW}$ (see Table 1). When comparing the nonpolar contribution among the three isoforms, we have found humC$\beta \approx$ humC$\alpha >$ rabFSk in loop 2 and humC$\beta >$ humC$\alpha >$ rabFSk in the CM loop (see Table 1), which contributes in part to the higher and lower actin binding affinity in humC$\beta$ and rabFSk, respectively. However, the nonpolar contribution of the HLH motif follows a different order [rabFSk $\approx$ humC$\alpha >$ humC$\beta$ (see Table 1)], which does not correlate with the order of actin binding affinity for these isoforms.

For electrostatic contribution $\Delta E_{elec}$, loops 2 and 3 contribute the most, followed by loop 4 and the CM loop, while the HLH motif contributes the least (see Table 1). The high electrostatic contribution from loop 2 is not entirely due to our modeling of loop 2 that optimizes the electrostatic interaction between loop 2 and AC3 (see Methods), because such interaction is free to break and form during the MD simulations and would not have persisted unless it is thermodynamically stable. When comparing the electrostatic contribution among the three isoforms, we have found humC$\beta >$ humC$\alpha >$ rabFSk in loop 2 (see Table 1), which follows the same order as the total electrostatic contribution (see Figure 3). This finding supports the key role of loop 2 in differentiating the actin binding affinity among these isoforms, and it echoes an early study that found the enzymatic activities of myosin correlate with chimeric substitutions in loop 2.[77] In contrast, the electrostatic contribution of loop 3 or 4 or the CM loop follows a different order (see Table 1), which does not correlate with the order of actin binding affinity for these isoforms.

After combining the nonpolar and electrostatic contributions (see Methods), we have found the contributions to $\Delta G$ by individual actin-binding motifs follow the order HLH $\approx$ loop 2 $\approx$ CM loop $>$ loop 3 $>$ loop 4 (see Table 1). For the HLH motif, loop 2, and the CM loop, the nonpolar contribution is greater than the electrostatic contribution (see Table 1), which supports the importance of extensive atomic contacts at the actin−myosin interface to strong actin−myosin binding in the rigor state. The electrostatic contribution, although smaller, may play a critical role in tuning the isoform-dependent actin binding affinity. In support of our finding, a previous study found that moderate changes to the net charge ($\leq$2) of loop 2 had only a small effect on actin binding affinity.[78] Our finding of the importance of loop 2 and the CM loop to actin−myosin binding agrees with the previous findings that the truncation of loop 2 reduced the actin binding affinity of myosin II by >100-fold,[44] and the deletion of the CM loop abolished actin−myosin binding,[79] although it is possible that such changes in affinity might result from nonspecific effects of loop deletion (such as structural changes). In agreement with our finding, Onishi and Morales proposed, on the basis of functional and mutational studies,[80−82] that loops 3 and 4 are involved in weak actin−myosin binding (but not strong actin−myosin binding), while the HLH motif, loop 2, and the CM Loop are involved in the weak-to-strong binding transition.[82] In partial agreement with our finding, a dynamic docking study using resonance energy transfer data found strong interaction of the CM loop and HLH motif, and limited interaction of loops 2−4 with actin in the post-powerstroke (rigor-state or ADP-state) model.[48] The discrepancy between our finding and ref 48 with respect to loop 2 interaction may be due to the lack of explicit loop 2 modeling and the use of a different non-rigor-like myosin structure for docking in their modeling.[48]

To trace the structural origin of the differences described above in actin−myosin binding among the three myosin isoforms, we have compared the average structures of these isoforms calculated on the basis of the MD simulations (see Figure S3 of the Supporting Information). Encouragingly, the lysine-rich loop 2 is closer to the negatively charged N-terminal region of AC3 in humC$\beta$ and humC$\alpha$ than in rabFSk, which agrees with the finding humC$\beta \geq$ humC$\alpha >$ rabFSk for the contribution of loop 2 to $\Delta E_{elec}$ and $\Delta G$ (see Table 1). Additionally, the separation between the CM loop and AC3 follows the order humC$\beta <$ humC$\alpha <$ rabFSk, which is consistent with the finding humC$\beta >$ humC$\alpha >$ rabFSk for the contribution of the CM loop to $E_{vdW}$ and $\Delta G$ (see Table 1).

After assessing the involvement of various actin-binding motifs in actin−myosin binding, we have performed a more refined analysis of $\Delta G$ at the residue level of detail. To identify key myosin residues involved in actin−myosin binding, we have partitioned $\Delta G$ into contributions from individual myosin residues [denoted $\Delta G_n$ for residue $n$ (see Methods and Table 2)]. To fully sample the dynamic interactions between myosin and actin, these per-residue contributions are averaged over the last 2 ns of 10 MD trajectories for each system. By ranking the


dx.doi.org/10.1021/bi4006896 | Biochemistry 2013, 52, 8393−8405

**Table 2. Top Contributing Residues of Three Myosin Isoforms Involved in Actin−Myosin Binding**

| rabFSk | | | | | humC$\alpha$ | | | | | humC$\beta$ | | | | |
|---|---|---|---|---|---|---|---|---|---|---|---|---|---|---|
| residue | $\Delta G_n$(sd) | $E_{vdW,n}$ | $\Delta E_{elec,n}$ | | residue | $\Delta G_n$(sd) | $E_{vdW,n}$ | $\Delta E_{elec,n}$ | | residue | $\Delta G_n$(sd) | $E_{vdW,n}$ | $\Delta E_{elec,n}$ | |
| R372 (R369)[a] | −0.14 (0.14) | −1.12 | +0.21 | M[b] | P403 (P402) | −0.12 (0.09) | −0.83 | +0.07 | | E371 | −0.12 (0.21) | +0.53 | −1.35 | |
| R406 (R403) | −0.19 (0.07) | −0.83 | −0.41 | ME | R404 (R403) | −0.25 (0.08) | −0.94 | −0.70 | ME | P402 | −0.24 (0.07) | −1.61 | +0.11 | |
| V407 (V404) | −0.44 (0.14) | −2.38 | −0.46 | ME | V405 (V404) | −0.42 (0.16) | −2.14 | −0.55 | ME | R403 | −0.29 (0.16) | −1.29 | −0.57 | ME |
| K408 (K405) | −0.18 (0.13) | −0.22 | −0.96 | | K406 (K405) | −0.18 (0.13) | −0.29 | −0.87 | | V404 | −0.42 (0.16) | −2.04 | −0.66 | ME |
| V409 (V406) | −0.21 (0.11) | −1.36 | +0.02 | ME | V407 (V406) | −0.21 (0.13) | −1.27 | −0.07 | ME | K405 | −0.20 (0.11) | −0.57 | −0.71 | |
| E412 (E409) | −0.13 (0.08) | −0.68 | −0.15 | E | N409 (N408) | −0.13 (0.14) | −0.62 | −0.21 | | V406 | −0.29 (0.14) | −1.55 | −0.32 | ME |
| Y413 (Y410) | −0.57 (0.21) | −3.40 | −0.20 | E | E410 (E409) | −0.16 (0.09) | −0.83 | −0.20 | E | N408 | −0.19 (0.15) | −0.94 | −0.26 | |
| V414 (V411) | −0.22 (0.08) | −1.41 | +0.03 | ME | Y411 (Y410) | −0.66 (0.28) | −3.96 | −0.25 | E | E409 | −0.13 (0.10) | −0.76 | −0.09 | E |
| T415 (T412) | −0.37 (0.09) | −2.53 | +0.23 | M | V412 (V411) | −0.18 (0.08) | −1.19 | +0.04 | ME | Y410 | −0.66 (0.28) | −4.16 | −0.02 | E |
| K416 (K413) | −0.17 (0.11) | −1.20 | +0.13 | | T413 (T412) | −0.32 (0.14) | −2.20 | +0.15 | M | V411 | −0.20 (0.11) | −1.32 | +0.03 | ME |
| G417 (G414) | −0.10 (0.06) | −0.62 | −0.02 | | K414 (K413) | −0.23 (0.16) | −1.73 | +0.26 | | T412 | −0.35 (0.09) | −2.41 | +0.22 | M |
| Q422 (Q419) | −0.11 (0.07) | −0.69 | −0.03 | | Q420 (Q419) | −0.12 (0.08) | −0.70 | −0.04 | | K413 | −0.20 (0.11) | −1.31 | +0.05 | |
| P530 (P527) | −0.33 (0.08) | −2.08 | −0.01 | E | P528 (P527) | −0.29 (0.10) | −1.82 | −0.02 | E | G414 | −0.14 (0.08) | −0.91 | +0.05 | |
| M531 (M528) | −0.39 (0.12) | −2.38 | −0.07 | E | M529 (M528) | −0.36 (0.13) | −2.20 | −0.07 | E | Q415 | −0.13 (0.07) | −0.79 | −0.03 | |
| S535 (S532) | −0.12 (0.11) | −0.95 | +0.19 | ME | S533 (S532) | −0.16 (0.10) | −1.11 | +0.13 | ME | N416 | −0.13 (0.09) | −0.82 | +0.03 | |
| E538 (E535) | −0.12 (0.05) | −1.22 | +0.50 | | I534 (I533) | −0.12 (0.05) | −0.82 | +0.04 | | Q419 | −0.17 (0.08) | −1.04 | −0.06 | |
| E539 (E536) | −0.17 (0.22) | −1.73 | +0.66 | E | E536 (E535) | −0.12 (0.05) | −1.19 | +0.45 | | P527 | −0.32 (0.09) | −2.03 | +0.01 | E |
| M542 (M539) | −0.69 (0.18) | −4.41 | +0.04 | ME | E537 (E536) | −0.15 (0.14) | −1.50 | +0.54 | E | M528 | −0.41 (0.13) | −2.52 | −0.06 | E |
| F543 (F540) | −0.41 (0.31) | −2.65 | +0.06 | E | M540 (M539) | −0.64 (0.15) | −4.04 | −0.01 | ME | S532 | −0.18 (0.06) | −1.25 | +0.13 | ME |
| P544 (P541) | −0.44 (0.13) | −2.89 | +0.08 | E | F541 (F540) | −0.62 (0.25) | −4.02 | +0.09 | E | M539 | −0.69 (0.13) | −4.40 | +0.02 | ME |
| K545 (K542) | −0.46 (0.16) | −2.31 | −0.60 | | P542 (P541) | −0.36 (0.14) | −2.42 | +0.12 | E | F540 | −0.36 (0.31) | −2.31 | +0.03 | E |
| N553 | −0.11 (0.05) | −0.63 | −0.06 | | K543 (K542) | −0.55 (0.16) | −2.74 | −0.75 | | P541 | −0.41 (0.15) | −2.67 | +0.05 | E |
| K554 (K551) | −0.13 (0.06) | −0.65 | −0.16 | | M547 (M546) | −0.12 (0.10) | −0.75 | −0.04 | | K542 | −0.40 (0.20) | −1.15 | −1.44 | |
| K568 (K565) | −0.10 (0.06) | −0.59 | −0.06 | | K552 (K551) | −0.15 (0.05) | −0.59 | −0.38 | | M546 | −0.15 (0.10) | −0.90 | −0.04 | |
| K570 (R567) | −0.26 (0.24) | +0.02 | −1.74 | E | K566 (K565) | −0.11 (0.06) | −0.58 | −0.13 | | K551 | −0.16 (0.05) | −0.71 | −0.28 | |
| P571 | −0.35 (0.16) | −2.35 | +0.11 | | R568 (R567) | −0.32 (0.24) | −0.46 | −1.63 | E | R567 | −0.31 (0.24) | +0.12 | −2.13 | E |
| K573 (K570) | −0.35 (0.23) | −0.63 | −1.67 | E | N569 (N568) | −0.25 (0.09) | −1.74 | +0.15 | | N568 | −0.31 (0.16) | −2.15 | +0.19 | |
| R574 | −0.11 (0.15) | +0.24 | −0.98 | | K571 (K570) | −0.21 (0.21) | +0.13 | −1.48 | E | K570 | −0.20 (0.19) | +0.17 | −1.50 | E |
| K637 | −0.16 (0.16) | −0.45 | −0.54 | | K635 (K633) | −0.12 (0.15) | −0.44 | −0.34 | | K633 | −0.28 (0.22) | −0.11 | −1.70 | |
| K638 (K635) | −0.29 (0.25) | −0.46 | −1.41 | | K637 (K635) | −0.37 (0.25) | −0.95 | −1.41 | | K635 | −0.14 (0.12) | −0.57 | −0.32 | |
| G639 (G636) | −0.11 (0.12) | −0.60 | −0.07 | | G638 (G636) | −0.16 (0.11) | −0.95 | −0.04 | | G636 | −0.14 (0.10) | −0.88 | −0.03 | |
| G640 | −0.12 (0.11) | −0.73 | −0.03 | | G639 | −0.16 (0.11) | −0.94 | −0.08 | | K637 | −0.52 (0.21) | −1.40 | −1.93 | ME |
| K641 | −0.25 (0.22) | −0.93 | −0.64 | | K640 | −0.24 (0.20) | −0.67 | −0.91 | | A638 | −0.24 (0.09) | −1.39 | −0.14 | |
| K642 (K639) | −0.24 (0.10) | −1.32 | −0.23 | E | K641 (K639) | −0.29 (0.16) | −1.62 | −0.24 | E | K639 | −0.27 (0.17) | −1.56 | −0.19 | E |
| K643 (K640) | −0.79 (0.25) | −4.22 | −0.83 | E | K642 (K640) | −0.94 (0.28) | −4.90 | −1.08 | E | K640 | −0.75 (0.33) | −3.61 | −1.14 | E |
| G644 (G641) | −0.23 (0.09) | −1.50 | +0.07 | | G643 (G641) | −0.33 (0.11) | −2.12 | −0.00 | | G641 | −0.19 (0.07) | −1.35 | +0.14 | |
| S645 (S642) | −0.11 (0.09) | −0.70 | +0.03 | M | S644 (S642) | −0.20 (0.07) | −1.29 | +0.05 | M | S642 | −0.27 (0.10) | −1.73 | +0.03 | M |
| F647 (F644) | −0.65 (0.27) | −4.20 | +0.10 | | S645 (S643) | −0.14 (0.07) | −0.97 | +0.06 | | S643 | −0.20 (0.07) | −1.36 | +0.09 | |
| Q648 (Q645) | −0.12 (0.07) | −0.76 | +0.03 | | F646 (F644) | −0.63 (0.17) | −4.04 | +0.07 | | F644 | −0.62 (0.18) | −4.01 | +0.11 | |

[a]For selected residues of humC$\alpha$ and rabFSk, the corresponding residue numbers of humC$\beta$ are shown in parentheses. [b]M means linked to HCM mutation, and E means experimentally tested.



dx.doi.org/10.1021/bi4006896 | Biochemistry 2013, 52, 8393−8405

per-residue contributions, we have selected 39 top contributing residues of myosin (see Table 2), which are primarily distributed in loop 2, the CM loop, and the HLH motif, with a few in loops 3 and 4.

Many of these actin-binding residues were validated as being functionally important by past mutational studies (see Table 2). In chicken smooth muscle myosin, the following mutations were found to compromise actin-activated ATPase: I407A, D412A, and V414A in the CM loop (corresponding to V404, E409, and V411, respectively, in humC$\beta$), K652A and K653A in loop 2 (corresponding to K639 and K640, respectively, in humC$\beta$), and W546A, F547A, and P548A (corresponding to M539, F540, and P541, respectively, in humC$\beta$).[80,81] A mutational study of V534, F535, and P536 in *Dictyostelium* myosin (corresponding to M539, F540, and P541, respectively, in humC$\beta$) also supported their importance for strong actin binding.[83] Mutation E531Q in *Dictyostelium* myosin (corresponding to E536 in humC$\beta$) was found to impair actin-activated ATPase and strong actin binding in the absence of ATP.[84]

Some of these residues are involved in mutations that cause HCM[7] (see Table 2), which are distributed over the following actin-binding motifs: R403, V404, V406, V411, and T412 in the CM loop, S532 and M539 in the HLH motif, and K637 and S642 in loop 2. In particular, the R403Q mutation in humC$\beta$ causes a severe form of HCM[85] and was found by *in vitro* analysis to be defective in actin binding.[86,87] Our finding that R403 directly contributes to actin−myosin binding differs from the previous finding by shorter MD simulations that R403 is indirectly involved in actin−myosin binding by forming an internal salt bridge with E605[37] or E631.[32]

Encouraged by the agreement with mutational data described above, we believe the remaining unexplored residues predicted in Table 2 will make promising targets for future mutational studies.

By comparing the predicted acin-binding residues and their contributions between humC$\beta$ and the other two isoforms (see Table 2), we have found seven humC$\beta$-specific actin-binding residues (P402, G414, Q415, and N416 in the CM loop and K633, K637, and A638 in loop 2). In particular, N416, K637, and A638 are not conserved between humC$\alpha$ and humC$\beta$ but are conserved within each family.[10] Therefore, these residues may contribute to the observed differences in actin−myosin binding affinity between humC$\beta$ and the other isoforms (see Methods). Interestingly, K637 is involved in a HCM-causing mutation.[7]

**Analysis of Electrostatic Interactions between Actin and Myosin.** Having established the importance of electrostatic interactions in tuning isoform-dependent actin−myosin binding, we have further explored the atomic details of these interactions. To this end, we have analyzed the occupancy of the hydrogen bonds (HBs) and salt bridges (SBs) dynamically formed at the actin−myosin interface during the last 2 ns of 10 MD simulations for humC$\beta$, humC$\alpha$, and rabFSk (see Methods). In support of the dynamic nature of actin−myosin interactions, the occupancy of individual HBs varies widely between 0 and 1, which seems to correlate negatively with the average donor−acceptor distances and their sd (see Figure S4 of the Supporting Information); the latter is linked to the dynamic fluctuations at the actin−myosin interface.

The number of HBs between AC1 or AC3 and myosin fluctuates significantly during MD simulations [varying in the ranges of 14−45, 14−37, and 10−30 for humC$\beta$, humC$\alpha$, and rabFSk (see Figure 4)], which supports the dynamic nature of electrostatic interactions at the actin−myosin interface.

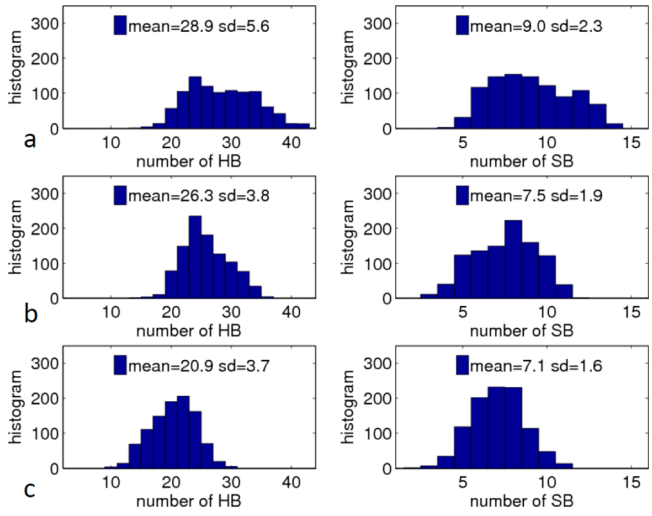


**Figure 4.** Distribution of the number of actin−myosin HBs and SBs for (a) humC$\beta$, (b) humC$\alpha$, and (c) rabFSk. The HB and SB analyses are performed for 1000 frames taken from the last 2 ns of 10 MD simulations for each system; the mean and standard deviation (sd) are shown for each distribution.

Interestingly, the number of actin−myosin HBs follows distinct distributions in the three myosin isoforms (see Figure 4). The average number of HBs follows the order humC$\beta$ > humC$\alpha$ > rabFSk (see Figure 4), which is the same as the order of electrostatic contribution to $\Delta G$ for these isoforms (see Figure 3). We have found a similar isoform dependence in the number of SBs between AC1 or AC3 and these myosin isoforms (see Figure 4). Despite large fluctuations in the number of HBs and SBs as indicated by their large sd (see Figure 4), these differences between isoforms are statistically significant because of greatly reduced standard errors ($\sim$sd/$\sqrt{1000}$ due to averaging over 1000 structural frames). Taken together, these findings support the importance of electrostatic interactions in differentiating the isoform-dependent actin binding affinity in the order humC$\beta$ > humC$\alpha$ > rabFSk. In addition to the higher number of HBs and SBs, humC$\beta$ also exhibits a greater variation in the number of HBs and SBs (see Figure 4), which indicates enhanced dynamics in the forming and breaking of HBs and SBs between AC1 or AC3 and humC$\beta$, although the backbone flexibility of actin-binding loops in humC$\beta$ is lower compared to that of rabFSk (see Figure 2).

We have analyzed all residue pairs that form transient actin−myosin HBs during the last 2 ns of MD simulations and then calculated the occupancy of each pair (see Methods). We focus on a subset of HB-forming residue pairs with an occupancy of $\geq$0.3, which are predicted to be important for the electrostatic interactions between AC1 or AC3 and myosin (see Table 3 and Movie S2 of the Supporting Information). These "high-occupancy" HB-forming residue pairs involve myosin residues from all five actin-binding motifs [loops 2−4, CM loop, and HLH motif (see Movie S2 of the Supporting Information)]. When comparing the three myosin isoforms, we have found more residue pairs forming high-occupancy HBs in humC$\beta$ than in humC$\alpha$ and rabFSk, especially in loop 2 and the CM loop (see Table 3). In humC$\beta$, six residue pairs form high-occupancy HBs between residues D628, K633, G636, K637,


dx.doi.org/10.1021/bi4006896 | *Biochemistry* 2013, 52, 8393−8405

**Table 3. Residue Pairs between Myosin and Actin Involved in High-Occupancy HBs**

| rabFSk | | | humC$\alpha$ | | | humC$\beta$ | | |
|---|---|---|---|---|---|---|---|---|
| myosin | actin | occupancy | myosin | actin | occupancy | myosin | actin | occupancy |
| E373 (E370)[a] | AC3:K328 | 0.63 | E371 (E370) | AC3:K328 | 1.17 | E370 | AC3:K328 | 0.57 |
| E374 (E371) | AC3:R147 | 2.48 | E372 (E371) | AC3:R147 | 2.61 | E371 | AC3:R147 | 2.26 |
| E374 (E371) | AC3:K328 | 0.41 | V405 (V404) | AC3:E334 | 0.84 | E371 | AC3:K328 | 0.33 |
| V407 (V404) | AC3:E334 | 0.82 | K406 (K405) | AC3:E334 | 0.67 | R403 | AC3:E334 | 0.31 |
| K408 (K405) | AC3:E334 | 0.73 | K406 (K405) | AC3:K336 | 0.49 | V404 | AC3:E334 | 0.83 |
| K408 (K405) | AC3:K336 | 0.57 | N409 (N408) | AC3:K336 | 0.46 | K405 | AC3:E334 | 0.92 |
| N411 (N408) | AC3:K336 | 0.44 | Y411 (Y410) | AC3:E334 | 0.77 | K405 | AC3:K336 | 0.34 |
| Y413 (Y410) | AC3:E334 | 0.73 | T413 (T412) | AC3:E334 | 0.32 | V406 | AC3:K336 | 0.42 |
| T415 (T412) | AC3:E334 | 0.31 | S533 (S532) | AC3:S350 | 0.34 | N408 | AC3:K336 | 0.46 |
| M531 (M528) | AC3:T351 | 0.34 | E537 (E536) | AC3:T351 | 0.77 | Y410 | AC3:E334 | 0.38 |
| S535 (S532) | AC3:S350 | 0.36 | D555 (D554) | AC1:K50 | 0.80 | K413 | AC3:A331 | 0.30 |
| E539 (E536) | AC3:T351 | 0.51 | R568 (R567) | AC1:E99 | 1.58 | E536 | AC3:T351 | 0.89 |
| E557 (D554) | AC1:K50 | 0.92 | R568 (R567) | AC1:E100 | 0.40 | K542 | AC1:E57 | 0.37 |
| K570 (R567) | AC1:D1 | 0.35 | K571 (K570) | AC1:E2 | 0.42 | K542 | AC3:E167 | 1.06 |
| K570 (R567) | AC1:E100 | 0.59 | E575 (E574) | AC1:R95 | 2.85 | R567 | AC1:D1 | 0.41 |
| K573 (K570) | AC1:E2 | 0.52 | E604 (E603) | AC3:R335 | 1.77 | R567 | AC1:E99 | 1.19 |
| K573 (K570) | AC1:E100 | 0.46 | D629 (D628) | AC3:R28 | 0.94 | R567 | AC1:E100 | 0.67 |
| R574 () | AC1:D1 | 0.64 | K637 (K635) | AC3:D3 | 0.34 | K570 | AC1:E2 | 0.36 |
| R574 () | AC1:E2 | 0.39 | K640 () | AC3:E2 | 0.39 | K570 | AC1:D3 | 0.49 |
| E577 (E574) | AC1:R95 | 2.05 | K642 (K640) | AC3:E4 | 0.54 | E574 | AC1:R95 | 3.05 |
| E606 (E603) | AC3:R335 | 0.44 | K642 (K640) | AC3:A7 | 0.72 | E603 | AC3:R335 | 2.76 |
| E633 () | AC3:R95 | 0.54 | | | | D628 | AC3:R28 | 1.05 |
| K638 (K635) | AC3:D3 | 0.31 | | | | K633 | AC3:E2 | 0.47 |
| | | | | | | G636 | AC3:D3 | 0.42 |
| | | | | | | K637 | AC3:E4 | 0.90 |
| | | | | | | A638 | AC3:E4 | 0.72 |
| | | | | | | K640 | AC3:E4 | 0.50 |

[a]For selected residues of humC$\alpha$ and rabFSk, the corresponding residue numbers of humC$\beta$ are shown in parentheses.

**Table 4. Residue Pairs between Myosin and Actin Involved in High-Occupancy SBs**

| rabFSk | | | humC$\alpha$ | | | humC$\beta$ | | |
|---|---|---|---|---|---|---|---|---|
| myosin | actin | occupancy | myosin | actin | occupancy | myosin | actin | occupancy |
| E373 (E370)[a] | AC3:K328 | 0.46 | E371 (E370) | AC3:K328 | 0.78 | E370 | AC3:K328 | 0.46 |
| E374 (E371) | AC3:R147 | 0.79 | E372 (E371) | AC3:R147 | 0.85 | E371 | AC3:R147 | 0.78 |
| E374 (E371) | AC3:K328 | 0.40 | D555 (D554) | AC3:K50 | 0.60 | K542 | AC3:E167 | 0.77 |
| E557 (D554) | AC3:K50 | 0.72 | R568 (R567) | AC3:E99 | 0.48 | R567 | AC3:E99 | 0.33 |
| K570 (R567) | AC3:D1 | 0.30 | K571 (K570) | AC3:E2 | 0.35 | K570 | AC3:E2 | 0.35 |
| K570 (R567) | AC3:E100 | 0.45 | E575 (E574) | AC3:R95 | 0.92 | K570 | AC3:D3 | 0.32 |
| K573 (K570) | AC3:E2 | 0.46 | E604 (E603) | AC3:R335 | 0.58 | E574 | AC3:R95 | 0.97 |
| K573 (K570) | AC3:E100 | 0.30 | K642 (K640) | AC3:E4 | 0.39 | E603 | AC3:R335 | 0.91 |
| E577 (E574) | AC3:R95 | 0.64 | | | | D628 | AC3:R28 | 0.34 |
| | | | | | | K633 | AC3:E2 | 0.40 |
| | | | | | | K637 | AC3:E4 | 0.75 |
| | | | | | | K640 | AC3:E4 | 0.47 |

[a]For selected residues of humC$\alpha$ and rabFSk, the corresponding residue numbers of humC$\beta$ are shown in parentheses.

A638, and K640 of loop 2 and residues E2, D3, E4, and R28 of AC3; eight residue pairs form high-occupancy HBs between R403, V404, K405, V406, N408, Y410, and K413 of the CM loop and residues A331, E334, and K336 of AC3 (see Movie S2 of the Supporting Information). In particular, two HB-forming residue pairs involving loop 2 (K637−E4 and A638−E4) are unique to humC$\beta$ and not present in humC$\alpha$ or rabFSk (see Table 3), and two residue pairs involving loop 2 (K633−E2 and G636−D3) have a much higher occupancy in humC$\beta$ than in humC$\alpha$ or rabFSk (see Table 3). This is in agreement with our finding that the electrostatic contribution of loop 2 to $\Delta G$ follows the order humC$\beta$ > humC$\alpha$ > rabFSk (see Table 1).

Some of the HBs identified here were also found by previous MD simulations and EM-based modeling of actin−myosin interactions.[31,32,37] For example, three HB-forming residue pairs between loop 4 and AC3 (E370−K328, E371−R147, and E371−K328) were observed in ref 37, two HB-forming residue pairs between the HLH motif and AC3 (E536−T351 and K542−E167) were observed in ref 32, and two HB-forming residue pairs between loop 3 and AC1 (R567−E100 and E574−R95) were observed in ref 31.

However, the loop 2 conformations and interactions observed in our MD simulations are different from those described in refs 32 and 37, where loop 2 was packed adjacent


dx.doi.org/10.1021/bi4006896 | Biochemistry 2013, 52, 8393−8405

to the CM loop and residues 23−25 of AC3, rather than extending to interact with the N-terminal segment of AC3 as observed in this study. Our simulations are more consistent with the experimental evidence for the involvement of the N-terminal segment of actin in actin−myosin binding.[45−47] Similar to our finding, in a recent EM-based study,[31] loop 2 of myosin I was found to form HBs with the N-terminal region of AC3. Future cross-linking experiments will be needed to validate these predicted interactions.

Similarly, we have analyzed a subset of residue pairs that form actin−myosin SBs with an occupancy of ≥0.3 (see Table 4). These high-occupancy SB-forming residue pairs involve myosin residues from loops 2−4 and the HLH motif (see Table 4). We have found more residue pairs forming high-occupancy SBs in humC$\beta$ than in humC$\alpha$ and rabFSk, especially in loop 2 (see Table 4): in humC$\beta$, four residue pairs form SBs between loop 2 and residues E2, E4, and R28 of AC3; in contrast, in rabFSk, no SB forms between loop 2 and AC3. A recent EM-fitting study also found two SBs between loop 2 of myosin I (residues K556 and K557) and N-terminal residues D1 and E2 of AC3.[31]

In summary, our analysis of HBs and SBs between myosin and AC1 or AC3 supports the importance of loop 2 in differentiating the actin binding affinity among humC$\beta$, humC$\alpha$, and rabFSk. In addition, our finding has substantiated, with atomic details, the putative actin−myosin contacts proposed on the basis of early EM studies:[88] contacts between loop 2 and actin residues 1−4, 24, and 25; contacts between the CM loop and actin residues 332−334; and contacts between loop 3 and actin residues 95−100.

**Discussion of How Actin Binding Affinity Depends on Differences in Sequence between humC$\beta$ and humC$\alpha$.** A recent sequence alignment of various $\alpha$- and $\beta$-isoforms of cardiac myosin found 40 conserved differences in the motor domain, which may be responsible for the kinetic differences between these two isoforms.[10] Some of these differences are in actin-binding motifs, particularly in the CM loop (such as N416S) and loop 2 (such as K637G and A638K), where isoform-dependent contributions to $\Delta G$ have been found in this study (see Table 2). Pervious experiments have explored the role of loop 2 and other regions in differentiating the kinetic properties of C$\alpha$ and C$\beta$ myosin. In one study,[12] chimeric myosins in which the sequences of either loop 1 and loop 2 or loop 2 of C$\alpha$ myosin were exchanged for those of C$\beta$ myosin were found to exhibit 2-fold differences in ATPase activity. In another study,[11] a chimeric myosin was created containing C$\beta$ sequence from residue 417 to 682 (including loop 2) within the C$\alpha$ backbone, which conferred C$\beta$-like actin-activated ATPase activity to the chimeric myosin. More specific mutational studies are needed to determine which residue differences in loop 2 lead to different actin binding affinity between humC$\beta$ and humC$\alpha$. It is conceivable that other residue differences far from the actin−myosin interface may play some roles in differentiating the kinetic properties between C$\alpha$ and C$\beta$ myosin (for example, by affecting the communication between the actin- and ATP-binding site), which is beyond the scope of this work.

## CONCLUSION

In summary, we have employed molecular modeling and simulations to investigate, with atomistic details, the isoform dependence of actin−myosin interactions in the rigor state. By combining electron microscopy-based docking with homology modeling, we have constructed three all-atom models for human cardiac $\alpha$ and $\beta$ and rabbit fast skeletal muscle myosin in complex with three actin subunits in the rigor state. Starting from these models, we have performed extensive all-atom MD simulations (total of 100 ns per system) and then used the MD trajectories to calculate the actin−myosin binding free energy with contributions from both electrostatic and nonpolar forces. Our binding calculations are in good agreement with the experimental finding of isoform-dependent differences in actin binding affinity between these myosin isoforms. Such differences are traced to changes in actin−myosin electrostatic interactions (i.e., hydrogen bonds and salt bridges) that are highly dynamic and involve several flexible actin-binding loops (such as loop 2). By partitioning the actin−myosin binding free energy to individual myosin residues, we have also identified key myosin residues involved in the actin−myosin interactions, some of which were previously validated experimentally or implicated in cardiomyopathy mutations, and the rest make promising targets for future mutational experiments.

As a final note, we emphasize that our modeling and simulation is based on the hypothesis that strong electrostatic interactions are formed between loop 2 of myosin and the N-terminal residues of actin (see Methods). Therefore, we cannot rule out alternative explanations for the differences in actin binding affinity between the myosin isoforms mentioned above if different models of loop 2 and other actin-binding motifs were to be constructed. Additionally, although our 10 ns MD simulations are more extensive than previous simulations, they remain relatively short compared with the functionally relevant time scales for actin−myosin binding, and longer simulations will be needed to assess the convergence of our results, which will be pursued in the future.

## ASSOCIATED CONTENT

### Supporting Information

Residue numbers of five actin-binding motifs in four myosin isoforms (Table S1), comparison of quality between rigid fitting and flexible fitting of actin and myosin into the EM map (Table S2), average rmsd values for myosin and actin (Table S3), results of convergence analysis (Table S4), rigid fitting of five actin subunits and the chkFSk myosin motor domain into the 13 Å EM map of myosin-decorated F-actin (Figure S1), rmsd values as a function of time for MD simulations of three myosin isoforms (Figure S2), comparison of average structures of three myosin isoforms bound with two actin subunits (Figure S3), occupancy of all actin−humC$\beta$ HBs plotted against the average and standard deviation of donor−acceptor distance (Figure S4), structural variations in the MD-generated ensemble of humC$\beta$ bound with two actin subunits (Movie S1), and high-occupancy HBs formed between two actin subunits and humC$\beta$ (Movie S2). This material is available free of charge via the Internet at http://pubs.acs.org.

## AUTHOR INFORMATION

### Corresponding Author

*E-mail: wjzheng@buffalo.edu. Telephone: (716) 645-2947. Fax: (716) 645-2507.

### Funding

Supported by the American Heart Association (Grant 0835292N) and the National Science Foundation (Grant 0952736).

### Notes

The authors declare no competing financial interest.

## ■ ACKNOWLEDGMENTS

The computer simulations were conducted using the supercomputing cluster of the Center for Computational Research at the University at Buffalo.

## ■ ABBREVIATIONS

CM loop, cardiomyopathy loop; chkFSk, chicken fast skeletal muscle myosin; CC, cross-correlation coefficient; EM, electron microscopy; humC$\alpha$, human cardiac $\alpha$ myosin; humC$\beta$, human cardiac $\beta$ myosin; HB, hydrogen bond; HCM, hypertrophic cardiomyopathy; MD, molecular dynamics; PDB, Protein Data Bank; rabFSk, rabbit fast skeletal muscle myosin; rmsd, root-mean-square deviation; rmsf, root-mean-square fluctuation; SB, salt bridge; sd, standard deviation.

## ■ REFERENCES

(1) Berg, J. S., Powell, B. C., and Cheney, R. E. (2001) A millennial myosin census. *Mol. Biol. Cell 12*, 780−794.
(2) Geeves, M. A., and Holmes, K. C. (1999) Structural mechanism of muscle contraction. *Annu. Rev. Biochem. 68*, 687−728.
(3) Spudich, J. A. (2001) The myosin swinging cross-bridge model. *Nat. Rev. Mol. Cell Biol. 2*, 387−392.
(4) Tyska, M. J., and Warshaw, D. M. (2002) The myosin power stroke. *Cell Motil. Cytoskeleton 51*, 1−15.
(5) De La Cruz, E. M., and Ostap, E. M. (2004) Relating biochemistry and function in the myosin superfamily. *Curr. Opin. Cell Biol. 16*, 61−67.
(6) Moore, J. R., Leinwand, L., and Warshaw, D. M. (2012) Understanding cardiomyopathy phenotypes based on the functional impact of mutations in the myosin motor. *Circ. Res. 111*, 375−385.
(7) Buvoli, M., Hamady, M., Leinwand, L. A., and Knight, R. (2008) Bioinformatics assessment of $\beta$-myosin mutations reveals myosin's high sensitivity to mutations. *Trends Cardiovasc. Med. 18*, 141−149.
(8) Miyata, S., Minobe, W., Bristow, M. R., and Leinwand, L. A. (2000) Myosin heavy chain isoform expression in the failing and nonfailing human heart. *Circ. Res. 86*, 386−390.
(9) Nakao, K., Minobe, W., Roden, R., Bristow, M. R., and Leinwand, L. A. (1997) Myosin heavy chain gene expression in human heart failure. *J. Clin. Invest. 100*, 2362−2370.
(10) Deacon, J. C., Bloemink, M. J., Rezavandi, H., Geeves, M. A., and Leinwand, L. A. (2012) Identification of functional differences between recombinant human $\alpha$ and $\beta$ cardiac myosin motors. *Cell. Mol. Life Sci. 69*, 2261−2277.
(11) Krenz, M., Sadayappan, S., Osinska, H. E., Henry, J. A., Beck, S., Warshaw, D. M., and Robbins, J. (2007) Distribution and structure-function relationship of myosin heavy chain isoforms in the adult mouse heart. *J. Biol. Chem. 282*, 24057−24064.
(12) Krenz, M., Sanbe, A., Bouyer-Dalloz, F., Gulick, J., Klevitsky, R., Hewett, T. E., Osinska, H. E., Lorenz, J. N., Brosseau, C., Federico, A., Alpert, N. R., Warshaw, D. M., Perryman, M. B., Helmke, S. M., and Robbins, J. (2003) Analysis of myosin heavy chain functionality in the heart. *J. Biol. Chem. 278*, 17466−17474.
(13) Fisher, A. J., Smith, C. A., Thoden, J. B., Smith, R., Sutoh, K., Holden, H. M., and Rayment, I. (1995) X-ray structures of the myosin motor domain of *Dictyostelium discoideum* complexed with MgADP·$BeF_x$ and MgADP·$AlF_4$. *Biochemistry 34*, 8960−8972.
(14) Rayment, I., Rypniewski, W. R., Schmidt-Base, K., Smith, R., Tomchick, D. R., Benning, M. M., Winkelmann, D. A., Wesenberg, G., and Holden, H. M. (1993) Three-dimensional structure of myosin subfragment-1: A molecular motor. *Science 261*, 50−58.
(15) Smith, C. A., and Rayment, I. (1996) X-ray structure of the magnesium(II)·ADP·vanadate complex of the *Dictyostelium discoideum* myosin motor domain to 1.9 Å resolution. *Biochemistry 35*, 5404−5417.
(16) Dominguez, R., Freyzon, Y., Trybus, K. M., and Cohen, C. (1998) Crystal structure of a vertebrate smooth muscle myosin motor domain and its complex with the essential light chain: Visualization of the pre-power stroke state. *Cell 94*, 559−571.
(17) Houdusse, A., Szent-Gyorgyi, A. G., and Cohen, C. (2000) Three conformational states of scallop myosin S1. *Proc. Natl. Acad. Sci. U.S.A. 97*, 11238−11243.
(18) Coureux, P. D., Sweeney, H. L., and Houdusse, A. (2004) Three myosin V structures delineate essential features of chemo-mechanical transduction. *EMBO J. 23*, 4527−4537.
(19) Coureux, P. D., Wells, A. L., Menetrey, J., Yengo, C. M., Morris, C. A., Sweeney, H. L., and Houdusse, A. (2003) A structural state of the myosin V motor without bound nucleotide. *Nature 425*, 419−423.
(20) Reubold, T. F., Eschenburg, S., Becker, A., Kull, F. J., and Manstein, D. J. (2003) A structural model for actin-induced nucleotide release in myosin. *Nat. Struct. Biol. 10*, 826−830.
(21) Yang, Y., Gourinath, S., Kovacs, M., Nyitray, L., Reutzel, R., Himmel, D. M., O'Neall-Hennessey, E., Reshetnikova, L., Szent-Gyorgyi, A. G., Brown, J. H., and Cohen, C. (2007) Rigor-like structures from muscle myosins reveal key mechanical elements in the transduction pathways of this allosteric motor. *Structure 15*, 553−564.
(22) Holmes, K. C., Popp, D., Gebhard, W., and Kabsch, W. (1990) Atomic model of the actin filament. *Nature 347*, 44−49.
(23) Oda, T., Iwasa, M., Aihara, T., Maeda, Y., and Narita, A. (2009) The nature of the globular- to fibrous-actin transition. *Nature 457*, 441−445.
(24) Fujii, T., Iwane, A. H., Yanagida, T., and Namba, K. (2010) Direct visualization of secondary structures of F-actin by electron cryomicroscopy. *Nature 467*, 724−728.
(25) Rayment, I., Holden, H. M., Whittaker, M., Yohn, C. B., Lorenz, M., Holmes, K. C., and Milligan, R. A. (1993) Structure of the actin-myosin complex and its implications for muscle contraction. *Science 261*, 58−65.
(26) Schroder, R. R., Manstein, D. J., Jahn, W., Holden, H., Rayment, I., Holmes, K. C., and Spudich, J. A. (1993) Three-dimensional atomic model of F-actin decorated with *Dictyostelium* myosin S1. *Nature 364*, 171−174.
(27) Volkmann, N., Hanein, D., Ouyang, G., Trybus, K. M., DeRosier, D. J., and Lowey, S. (2000) Evidence for cleft closure in actomyosin upon ADP release. *Nat. Struct. Biol. 7*, 1147−1155.
(28) Volkmann, N., Liu, H., Hazelwood, L., Krementsova, E. B., Lowey, S., Trybus, K. M., and Hanein, D. (2005) The structural basis of myosin V processive movement as revealed by electron cryomicroscopy. *Mol. Cell 19*, 595−605.
(29) Holmes, K. C., Angert, I., Kull, F. J., Jahn, W., and Schroder, R. R. (2003) Electron cryo-microscopy shows how strong binding of myosin to actin releases nucleotide. *Nature 425*, 423−427.
(30) Holmes, K. C., Schroder, R. R., Sweeney, H. L., and Houdusse, A. (2004) The structure of the rigor complex and its implications for the power stroke. *Philos. Trans. R. Soc., B 359*, 1819−1828.
(31) Behrmann, E., Muller, M., Penczek, P. A., Mannherz, H. G., Manstein, D. J., and Raunser, S. (2012) Structure of the rigor actin-tropomyosin-myosin complex. *Cell 150*, 327−338.
(32) Lorenz, M., and Holmes, K. C. (2010) The actin-myosin interface. *Proc. Natl. Acad. Sci. U.S.A. 107*, 12529−12534.
(33) Yu, H., Ma, L., Yang, Y., and Cui, Q. (2007) Mechanochemical coupling in the myosin motor domain. I. Insights from equilibrium active-site simulations. *PLoS Comput. Biol. 3*, e21.
(34) Yu, H., Ma, L., Yang, Y., and Cui, Q. (2007) Mechanochemical coupling in the myosin motor domain. II. Analysis of critical residues. *PLoS Comput. Biol. 3*, e23.
(35) Yang, Y., Yu, H., and Cui, Q. (2008) Extensive conformational transitions are required to turn on ATP hydrolysis in myosin. *J. Mol. Biol. 381*, 1407−1420.
(36) Fischer, S., Windshugel, B., Horak, D., Holmes, K. C., and Smith, J. C. (2005) Structural mechanism of the recovery stroke in the myosin molecular motor. *Proc. Natl. Acad. Sci. U.S.A. 102*, 6873−6878.

(37) Liu, Y., Scolari, M., Im, W., and Woo, H. J. (2006) Protein-protein interactions in actin-myosin binding and structural effects of R405Q mutation: A molecular dynamics study. *Proteins 64*, 156−166.
(38) Zheng, W. (2010) Multiscale modeling of structural dynamics underlying force generation and product release in actomyosin complex. *Proteins 78*, 638−660.
(39) Lowey, S., Bretton, V., Gulick, J., Robbins, J., and Trybus, K. M. (2013) Transgenic Mouse $\alpha$- and $\beta$-Cardiac Myosins Containing the R403Q Mutation Show Isoform Dependent Transient Kinetic Differences. *J. Biol. Chem. 288*, 14780−14787.
(40) Sali, A., and Blundell, T. L. (1993) Comparative protein modelling by satisfaction of spatial restraints. *J. Mol. Biol. 234*, 779−815.
(41) Fiser, A., Do, R. K., and Sali, A. (2000) Modeling of loops in protein structures. *Protein Sci. 9*, 1753−1773.
(42) Eswar, N., Webb, B., Marti-Renom, M. A., Madhusudhan, M. S., Eramian, D., Shen, M. Y., Pieper, U., and Sali, A. (2006) Comparative protein structure modeling using Modeller. *Current protocols in bioinformatics*, Chapter 5, Unit 5, 6, Wiley, New York.
(43) Pettersen, E. F., Goddard, T. D., Huang, C. C., Couch, G. S., Greenblatt, D. M., Meng, E. C., and Ferrin, T. E. (2004) UCSF chimera: A visualization system for exploratory research and analysis. *J. Comput. Chem. 25*, 1605−1612.
(44) Knetsch, M. L., Uyeda, T. Q., and Manstein, D. J. (1999) Disturbed communication between actin- and nucleotide-binding sites in a myosin II with truncated 50/20-kDa junction. *J. Biol. Chem. 274*, 20133−20138.
(45) Miller, C. J., Wong, W. W., Bobkova, E., Rubenstein, P. A., and Reisler, E. (1996) Mutational analysis of the role of the N terminus of actin in actomyosin interactions. Comparison with other mutant actins and implications for the cross-bridge cycle. *Biochemistry 35*, 16557−16565.
(46) DasGupta, G., and Reisler, E. (1991) Nucleotide-induced changes in the interaction of myosin subfragment 1 with actin: Detection by antibodies against the N-terminal segment of actin. *Biochemistry 30*, 9961−9966.
(47) Sutoh, K. (1982) Identification of myosin-binding sites on the actin sequence. *Biochemistry 21*, 3654−3661.
(48) Root, D. D., Stewart, S., and Xu, J. (2002) Dynamic docking of myosin and actin observed with resonance energy transfer. *Biochemistry 41*, 1786−1794.
(49) Prochniewicz, E., and Thomas, D. D. (2001) Site-specific mutations in the myosin binding sites of actin affect structural transitions that control myosin binding. *Biochemistry 40*, 13933−13940.
(50) Feig, M., Karanicolas, J., and Brooks, C. L., III (2004) MMTSB Tool Set: Enhanced sampling and multiscale modeling methods for applications in structural biology. *J. Mol. Graphics Modell. 22*, 377−395.
(51) Humphrey, W., Dalke, A., and Schulten, K. (1996) VMD: Visual molecular dynamics. *J. Mol. Graphics 14*, 27−38.
(52) Martyna, G. J., Hughes, A., and Tuckerman, M. E. (1999) Molecular dynamics algorithms for path integrals at constant pressure. *J. Chem. Phys. 110*, 3275−3290.
(53) Deserno, M., and Holm, C. (1998) How to mesh up Ewald sums. I. A theoretical and numerical comparison of various particle mesh routines. *J. Chem. Phys. 109*, 7678−7693.
(54) Hoover, W. G. (1985) Canonical Dynamics: Equilibrium Phase-Space Distributions. *Phys. Rev. A 31*, 1695−1697.
(55) Phillips, J. C., Braun, R., Wang, W., Gumbart, J., Tajkhorshid, E., Villa, E., Chipot, C., Skeel, R. D., Kale, L., and Schulten, K. (2005) Scalable molecular dynamics with NAMD. *J. Comput. Chem. 26*, 1781−1802.
(56) MacKerell, A. D., Bashford, D., Bellott, M., Dunbrack, R. L., Evanseck, J. D., Field, M. J., Fischer, S., Gao, J., Guo, H., Ha, S., Joseph-McCarthy, D., Kuchnir, L., Kuczera, K., Lau, F. T. K., Mattos, C., Michnick, S., Ngo, T., Nguyen, D. T., Prodhom, B., Reiher, W. E., Roux, B., Schlenkrich, M., Smith, J. C., Stote, R., Straub, J., Watanabe, M., Wiorkiewicz-Kuczera, J., Yin, D., and Karplus, M. (1998) All-atom empirical potential for molecular modeling and dynamics studies of proteins. *J. Phys. Chem. B 102*, 3586−3616.
(57) Mackerell, A. D., Jr., Feig, M., and Brooks, C. L., III (2004) Extending the treatment of backbone energetics in protein force fields: Limitations of gas-phase quantum mechanics in reproducing protein conformational distributions in molecular dynamics simulations. *J. Comput. Chem. 25*, 1400−1415.
(58) Le, L., Lee, E., Schulten, K., and Truong, T. N. (2009) Molecular modeling of swine influenza A/H1N1, Spanish H1N1, and avian H5N1 flu N1 neuraminidases bound to Tamiflu and Relenza. *PLoS Currents 1*, RRN1015.
(59) Barlow, D. J., and Thornton, J. M. (1983) Ion-pairs in proteins. *J. Mol. Biol. 168*, 867−885.
(60) Li, M. H., and Zheng, W. J. (2011) Probing the Structural and Energetic Basis of Kinesin-Microtubule Binding Using Computational Alanine-Scanning Mutagenesis. *Biochemistry 50*, 8645−8655.
(61) Li, M., and Zheng, W. (2012) All-atom structural investigation of kinesin-microtubule complex constrained by high-quality cryo-electron-microscopy maps. *Biochemistry 51*, 5022−5032.
(62) Eriksson, M. A., and Roux, B. (2002) Modeling the structure of agitoxin in complex with the Shaker $K^+$ channel: A computational approach based on experimental distance restraints extracted from thermodynamic mutant cycles. *Biophys. J. 83*, 2595−2609.
(63) Gilson, M. K., and Honig, B. H. (1988) Energetics of charge-charge interactions in proteins. *Proteins 3*, 32−52.
(64) Im, W., Beglov, D., and Roux, B. (1998) Continuum Solvation Model: Computation of electrostatic forces from numerical solutions to the Poisson-Boltzmann equation. *Comput. Phys. Commun. 111*, 59−75.
(65) Kull, F. J., Sablin, E. P., Lau, R., Fletterick, R. J., and Vale, R. D. (1996) Crystal structure of the kinesin motor domain reveals a structural similarity to myosin. *Nature 380*, 550−555.
(66) Olson, M. A., and Reinke, L. T. (2000) Modeling implicit reorganization in continuum descriptions of protein-protein interactions. *Proteins 38*, 115−119.
(67) Gilson, M. K., and Honig, B. H. (1986) The dielectric constant of a folded protein. *Biopolymers 25*, 2097−2119.
(68) Sharp, K. A., and Honig, B. (1990) Electrostatic interactions in macromolecules: Theory and applications. *Annu. Rev. Biophys. Biophys. Chem. 19*, 301−332.
(69) Sharp, K. A., and Honig, B. (1990) Calculating Total Electrostatic Energies with the Nonlinear Poisson-Boltzmann Equation. *J. Phys. Chem. 94*, 7684−7692.
(70) Ritchie, M. D., Geeves, M. A., Woodward, S. K., and Manstein, D. J. (1993) Kinetic characterization of a cytoplasmic myosin motor domain expressed in *Dictyostelium discoideum*. *Proc. Natl. Acad. Sci. U.S.A. 90*, 8619−8623.
(71) Roux, B. (1997) Influence of the membrane potential on the free energy of an intrinsic protein. *Biophys. J. 73*, 2980−2989.
(72) Nina, M., Beglov, D., and Roux, B. (1997) Atomic radii for continuum electrostatics calculations based on molecular dynamics free energy simulations. *J. Phys. Chem. B 101*, 5239−5248.
(73) Brooks, B. R., Bruccoleri, R. E., Olafson, B. D., States, D. J., Swaminathan, S., and Karplus, M. (1983) Charmm: A Program for Macromolecular Energy, Minimization, and Dynamics Calculations. *J. Comput. Chem. 4*, 187−217.
(74) Stigler, S. (2008) Fisher and the 5% level. *CHANCE 21*, 12−12.
(75) Volkmann, N., Ouyang, G., Trybus, K. M., DeRosier, D. J., Lowey, S., and Hanein, D. (2003) Myosin isoforms show unique conformations in the actin-bound state. *Proc. Natl. Acad. Sci. U.S.A. 100*, 3227−3232.
(76) Kany, H., Wolf, J., and Kalbitzer, H. R. (2002) Myosin II from rabbit skeletal muscle and *Dictyostelium discoideum* and its interaction with F-actin studied by $^1$H NMR spectroscopy. *FEBS Lett. 521*, 121−126.
(77) Uyeda, T. Q., Ruppel, K. M., and Spudich, J. A. (1994) Enzymatic activities correlate with chimaeric substitutions at the actin-binding face of myosin. *Nature 368*, 567−569.

(78) Furch, M., Geeves, M. A., and Manstein, D. J. (1998) Modulation of actin affinity and actomyosin adenosine triphosphatase by charge changes in the myosin motor domain. *Biochemistry 37*, 6317−6326.
(79) Sasaki, N., Asukagawa, H., Yasuda, R., Hiratsuka, T., and Sutoh, K. (1999) Deletion of the myopathy loop of *Dictyostelium* myosin II and its impact on motor functions. *J. Biol. Chem. 274*, 37840−37844.
(80) Kojima, S., Konishi, K., Katoh, K., Fujiwara, K., Martinez, H. M., Morales, M. F., and Onishi, H. (2001) Functional roles of ionic and hydrophobic surface loops in smooth muscle myosin: Their interactions with actin. *Biochemistry 40*, 657−664.
(81) Onishi, H., Mikhailenko, S. V., and Morales, M. F. (2006) Toward understanding actin activation of myosin ATPase: The role of myosin surface loops. *Proc. Natl. Acad. Sci. U.S.A. 103*, 6136−6141.
(82) Onishi, H., and Morales, M. F. (2007) A closer look at energy transduction in muscle. *Proc. Natl. Acad. Sci. U.S.A. 104*, 12714−12719.
(83) Hachikubo, Y., Ito, K., and Yamamoto, K. (2003) Roles of the hydrophobic triplet in the motor domain of myosin in the interaction between myosin and actin. *J. Biochem. 134*, 165−171.
(84) Giese, K. C., and Spudich, J. A. (1997) Phenotypically selected mutations in myosin's actin binding domain demonstrate intermolecular contacts important for motor function. *Biochemistry 36*, 8465−8473.
(85) Geisterfer-Lowrance, A. A., Kass, S., Tanigawa, G., Vosberg, H. P., McKenna, W., Seidman, C. E., and Seidman, J. G. (1990) A molecular basis for familial hypertrophic cardiomyopathy: A $\beta$ cardiac myosin heavy chain gene missense mutation. *Cell 62*, 999−1006.
(86) Cuda, G., Fananapazir, L., Zhu, W. S., Sellers, J. R., and Epstein, N. D. (1993) Skeletal muscle expression and abnormal function of $\beta$-myosin in hypertrophic cardiomyopathy. *J. Clin. Invest. 91*, 2861−2865.
(87) Sweeney, H. L., Straceski, A. J., Leinwand, L. A., Tikunov, B. A., and Faust, L. (1994) Heterologous expression of a cardiomyopathic myosin that is defective in its actin interaction. *J. Biol. Chem. 269*, 1603−1605.
(88) Milligan, R. A. (1996) Protein-protein interactions in the rigor actomyosin complex. *Proc. Natl. Acad. Sci. U.S.A. 93*, 21−26.